Enhancements and Fermi surfaces of rare-earth hexaborides

1990 J. Phys.: Condens. Matter 2 559

(http://iopscience.iop.org/0953-8984/2/3/005)

J. Phys.: Condens. Matter **2** (1990) 559–575. Printed in the UK

Enhancements and Fermi surfaces of rare-earth hexaborides

H D Langford†, W M Temmerman‡ and G A Gehring†

† Department of Theoretical Physics, University of Oxford, 1 Keble Road, Oxford OX1 3NP, UK

‡ SERC Daresbury Laboratory, Warrington WA4 4AD, UK

Received 13 September 1989

Abstract. The properties of rare-earth hexaborides have been studied within the framework of density functional theory. The LMTO-ASA method has been used to study the electronic structure of paramagnetic LaB_6, CeB_6, PrB_6 and NdB_6 and of ferromagnetic CeB_6, PrB_6 and NdB_6. In the ferromagnetic case, which treats the f electrons as true band states, we find good quantitative agreement between the experimental and theoretical Fermi surfaces. In addition, comparison of spin moments and total energies is used to predict the zero-field susceptibility within a Landau free energy argument. This indicates that the experimentally heavy fermion system CeB_6 does indeed have a substantially enhanced effective electron mass.

1. Introduction

Much attention has recently been focused on the so-called heavy fermion systems. These systems are characterised by a large density of states at the Fermi energy which can be up to 1000 times that expected for a normal metal. This can be interpreted as a high effective electron mass.

Interest in these compounds was first aroused by measurement of the linear coefficient of specific heat $\gamma(0)$ (where $\gamma(T) = C(T)/T$) which is massively enhanced over that of a normal metal such as copper. A wide variety of ground states is also exhibited, with the notable possibility of exotic superconductivity, for example in UPt_3 (Stewart 1984, Stewart *et al* 1984).

Some understanding of the mechanism that gives rise to these strong enhancements has been achieved by analysis of the Periodic Anderson Model (Anderson 1961), a phenomenological model which describes localised f-electrons hybridising with the conduction band and experiencing a large on-site Coulomb correlation energy. The application of standard many-body techniques to this model can, among other things, qualitatively explain the large enhancement of $\gamma(0)$ (Rasul and Desgranges 1986). However, this approach which usually assumes an isotropic conduction band, cannot explain why $\gamma(T)$ is drastically different for different heavy fermion compounds, nor why different compounds should have such such different ground states (Stewart 1984). These facts must be in some way attributable to the detailed electronic structure of the system and any theory which aspires to give us a quantitative description needs to include

0953-8984/90/030559 + 17 $03.50

features as crystal structure effects, correct symmetry of band states, full orbital and spin degeneracy of the f states, dynamics of conduction electrons, Coulomb interactions and hybridisation of f states with conduction electrons, Luttinger's theorem constraints and spin-orbit coupling (Pickett 1986). This naturally leads to an attempt to analyse these systems with a fully self-consistent all electron band theory calculated using density functional theory (DFT) (Hohenberg and Kohn 1964), which approach can in principle include all the above effects that are usually disregarded in a model calculation.

The main drawbacks to the band theory approch using DFT are that only ground state properties are guaranteed and the exact exchange–correlation functional is unknown, necessitating the use of the local density approximation (LDA) (Kohn and Sham 1965) or the local spin density (LSD) (Gunnarsson and Lundqvist, 1976) approximation for spin-polarised calculations. These disadvantages preclude a full description of the strong f–f correlations, but on the other hand it is the only *ab initio* theory we have and can at least give information on approximate band placements and widths, etc., as well as an accurate picture of the one-electron electronic structure. Also, it provides a method for estimating quantitatively the magnitude of many-body enhancements, but the most important thing is that it is the only theory that can make any predictions about the detailed form of the Fermi surface in these materials. The Fermi surface is in principle measurable and great success has been achieved by comparing the experimental and theoretical Fermi surfaces for UPt_3 (Taillefer *et al* 1987, Oguchi and Freeman 1986, Wang *et al* 1987, Langford and Temmerman 1988, Christensen *et al* 1988). In spite of this, there is still controversy as to whether even exact DFT can give the correct quasiparticle Fermi surface, as compared to that calculated from the self-energy (Schönhammer and Gunnarsson 1988), although these arguments provide no indication as to how accurately the DFT Fermi surface approximates that of the quasiparticles.

In this paper we present a band theory study of the rare-earth hexaboride series ReB_6 (Re = La, Ce, Pr, Nd) with particular reference to the heavy fermion CeB_6. Experimentally, the phase diagram of CeB_6 ($\gamma(0) = 250$ mJ mol^{-1} K^{-2} (Bredl 1987)) is complex, with two phase transitions at $T_Q = 3.2$ K to an antiferroquadrupolar ordering and at $T_N = 2.4$ K to a double-k antiferromagnetic structure (Effantin *et al* 1985). The transition temperatures are strongly affected by the application of an external field, the antiferromagnetic ground state being destroyed by field above 1–2 T. NdB_6 is a simple antiferromagnet ($T_N = 8.5$ K) whilst PrB_6 is intermediate, ordering at $T_N = 6.9$ K into an incommensurate double-k structure and then at $T_C = 3.9$ K into a commensurate double-k structure (Burlet *et al* 1988). These properties must be due to exchange interactions, which increase from CeB_6 to PrB_6 and NdB_6. There has to be strong anisotropy to stabilise the double-k structure, which could arise from 4f conduction electron hybridisation. The magnetism competes with antiferroquadrupolar interactions, the latter being dominant in CeB_6, weaker in NdB_6 and intermediate in PrB_6. This rich variety of properties indicates that the detailed microscopic behaviour of the electrons is crucial, so this naturally leads to the need for a band theory analysis.

As magnetic interactions are obviously important, we have performed both paramagnetic and spin-polarised calculations in order to investigate the possibility of ferromagnetic ordering. We chose this as it is the simplest possible magnetic state, and, moreover, the antiferroquadrupolar, incommensurate and double-k orderings are beyond current band theory techniques, the first two for theoretical reasons and the last one for the computational problem of having 32 structural unit cells in the magnetic unit cell (Effantin *et al* 1985).

The aim of this paper is as follows. First, we shall discuss the charge densities, band placements and band splittings where appropriate to see how the extra f electron is

accommodated as we traverse the ReB_6 row. Then will come an analysis of the bands and Fermi surfaces, drawing on the experimenal result that a large portion of the Fermi surface of LaB_6 is at least qualitatively reproduced in the other three compounds. From this we will arrive at a detailed picture of the formation of the Fermi surface, and, more specifically, the role the f electrons play. Finally, there will be a discussion of the enhancements of the effective masses and low temperature specific heats over those calculated.

2. Details of the calculation

We have performed self-consistent electronic structure calculations for the rare-earth hexaborides ReB_6 (Re = La, Ce, Pr and Nd). These were standard DFT calculations using the Von Barth–Hedin approximation to the exchange and correlation energy in the LDA (von Barth and Hedin 1972). The band structure method employed was the linear muffin-tin orbital approach in the atomic sphere approximation (LMTO-ASA) (Andersen 1975, Skriver 1984). For LaB_6, spin–orbit coupling was included along with mass–velocity and Darwin terms in the iterations to self-consistency, while for the spin-polarised calculations, which use the LSD approximation to the exchange and correlation energy, a semi-relativistic formulation was used where spin–orbit coupling is neglected, but the other relativistic corrections are kept. (A paramagnetic calculation for CeB_6 which includes spin-orbit coupling has been reported elsewhere (Langford and Temmerman, 1988) and will be referred to in the text for the sake of comparison.)

These hexaborides have the well known CaB_6 crystal structure, which can be viewed as a CsCl structure with Ca atoms at the Cs sites and B octahedra at the Cl sites (Blum and Bertaut, 1954). We used the quoted lattice constants, i.e. $a = 4.156$ Å for LaB_6, $a = 4.141$ Å for CeB_6, $a = 4.121$ Å for PrB_6 and $a = 4{,}128$ Å for NdB_6. There are seven atoms per unit cell and, in the iterations to self-consistency, 84 k-points were sampled in 1/48th of the Brillouin zone.

The initial charge densities were chosen to be core + $2s^22p^1$ for B, core + $4f^05d^16s^2$ for La, core + $4f^15d^16s^2$ for Ce, core + $4f^25d^26s^2$ for Pr and core + $4f^35d^16s^2$ for Nd and a frozen-core approximation was used using one panel. (For technical reasons, this initial choice of parameters is crucial. The boron s and p electrons must be kept in the same panel, since they hybridise strongly to give a very different electron count to the free atom and we also found that, due to this strong boron s–p hybridisation, we could only use one panel, which necessitates keeping the rare-earth 5p electrons as part of the frozen core.)

3. Results

3.1. Charge and energy data and densities of states

Table 1 shows the charges, densities of states at the Fermi energy E_F, and band positions for the calculations on paramagnetic LaB_6 and CeB_6 that include spin–orbit coupling. It should be noticed that the charges are very similar apart from the lanthanide f charge differing by just over one. This result is non-trivial as it is not built into the calculation, the La f character originating from re-expansion of orbitals originating on other sites into $l = 3$ on the La site. The fact that the f charge is so large on the La site is due to the

Table 1. The charges, densities of states and band positions of paramagnetic LaB_6 and CeB_6 including spin–orbit coupling.

		CeB_6 (f core)		CeB_6 (f band)		LaB_6	
		Ce	B	Ce	B	La	B
ASA radius (au)		4.04	2.00796	4.04	2.00796	4.05464	2.01523
Electrons per atom	s	0.48	0.87	0.44	0.84	0.43	0.85
	p	0.99	1.94	0.94	1.88	0.92	1.89
	d	2.71		2.20		2.30	
	f	—		2.11		0.94	
Total charge per atom		4.19	2.81	5.69	2.72	4.59	2.74
$N(E_F)$ (states eV^{-1}/ cell)	s	0.01	0.02	0.01	0.02	0.00	0.01
	p	0.00	0.16	0.11	0.41	0.01	0.18
	d	0.42		0.48		0.38	
	f	—		8.93		0.14	
Total		0.43	0.18	9.53	0.43	0.53	0.19
Band centre relative to E_F (mRyd)	s	−325	−835	−222	−801	−233	−825
	p	+287	+138	+388	+168	384	+140
	d	−42		+74		+47	
	f	—		+26		+316	
$\gamma(0)$ in mJ mol^{-1} K^{-2}		1.4		23.4		1.7	

fact that the rare-earth Wigner–Seitz radius is much larger than that of the boron. We chose the Wigner–Seitz radii after a detailed calculation on the bonding properties of CeB_6 (Langford and Temmerman, 1988). We determined the necessary ASA sphere sizes required to give the correct lattice constant for that compound and then chose the radii of the other rare-earth and boron spheres for each subsequent compound to be in the same ratio as that determined for the cerium and boron spheres in CeB_6.

We see that in all calculations, the boron charge is such that there are roughly two p electrons and one s electron in contrast to the free atom. This is due to a very strong boron s–p hybridisation.

Table 2 shows corresponding results for semi-relativistic paramagnetic calculations on CeB_6, PrB_6 and NdB_6. Again we see that the f charge increases monotonically along the series such that the total rare-earth charge increases by one, leaving the boron almost unchanged. This result is useful because it is what we would expect physically and allows us to observe the systematic behaviour as we go across the ReB_6 row of compounds, adding one electron at a time to the rare-earth atom. Although the density of f states at the Fermi energy ($N_f(E_F)$) is erratic, we see that the s–p–d electron density of states gradually decreases across the Ce–Pr–Nd series, corresponding to a reduced amount of hybridisation between the f states, which are pinned to E_F, and the s–p–d states. To emphasise this point, observe that the main change in the positions of the band centres is an increased f–d separation as we go across the series, with an accompanying reduction of d charge on the rare-earth ion. This corresponds to increasing localisation of the f electrons as we go across the row of compounds.

Table 3 shows comparative results for the semi-relativistic spin-polarised calculations—all three compounds CeB_6, PrB_6 and NdB_6 do indeed form an energetically

Table 2. The charges, densities of states and band positions of paramagnetic CeB_6, PrB_6 and NdB_6.

		CeB_6		PrB_6		NdB_6	
		Ce	B	Pr	B	Nd	B
ASA radius (au)		4.04	2.00796	4.0205	1.9983	4.0277	2.00185
Electrons per atom	s	0.44	0.84	0.45	0.83	0.45	0.83
	p	0.94	1.88	0.95	1.88	0.96	1.87
	d	2.21		2.10		2.00	
	f	2.11		3.26		4.35	
Total charge per atom		5.70	2.72	6.75	2.71	7.76	2.71
$N(E_F)$ (states eV^{-1}/cell)	s	0.01	0.02	0.01	0.01	0.00	0.00
	p	0.11	0.38	0.09	0.39	0.01	0.13
	d	0.45		0.38		0.08	
	f	7.61		19.15		10.55	
Total		8.18	0.40	19.63	0.40	10.64	0.13
Band centre relative to E_F (mRyd)	s	−223	−801	−220	−790	−223	−782
	p	+387	+168	+392	+184	+379	+190
	d	+73		+102		+121	
	f	+21		+9		+3	
$\gamma(0)$ in mJ mol^{-1} K^{-2}		20.2		47.1		25.4	

stable magnetic ground state. Most of the moment resides in the f channel, as one would expect, with the d contribution becoming relatively less important as we go across the series. There is also a reduction in $N(E_F)$ as compared to the paramagnetic calculations. This is as one might expect, except in the case of NdB_6, where the precise value of $N(E_F)$ is extremely sensitive to the exact position of the Fermi energy. Band splittings are comparable along the row of compounds except for the f states, where the Ce f splitting is very much less than that of the other two, despite there being a very sizeable spin moment. This unique behaviour of the cerium is also illustrated in table 4 where the separate constituents of the total energy have been compared for the paramagnetic and spin-polarised calculations using the decomposition

$$E_{\text{Total}} = E_{\text{Band}} + E_{\text{XC}} + E_{\text{Coulomb}} + E_{\text{Mad}} \tag{1}$$

where the four terms on the right hand side are, respectively, the one-electron band energy, the exchange–correlation energy, the Coulomb energy and the Madelung contribution from the charged ASA spheres in each unit cell. It is immediately apparent that the formation of the magnetic ground state is a competition between raising the band energy by removing some electron states above the Fermi energy, whilst recovering this by lowering the Coulomb and exchange–correlation terms. Also, it is evident that the magnetic stabilisation energy of CeB_6 is relatively very small for such a large spin moment. Cobalt, for example, has a LSD spin moment of 1.56 μ_B and a stabilisation energy of 8 mRyd, iron a moment of 2.15 μ_B (21.5 mRyd) and nickel a moment of 0.59 μ_B (6 mRyd) (Moruzzi *et al* 1978). This must in some way mean that CeB_6 has an enhanced magnetic spin susceptibility, to which point we shall return in section 5. (It should be noted that these stabilisation energies and spin moments are not particularly sensitive to the number of k-points used in the Brillouin zone integration, as shown by a test run

Table 3. The charges, densities of states and band splittings of spin-polarised CeB_6, Prb_6 and NdB_6.

		CeB_6		PrB_6		NdB_6	
		Ce	B	Pr	B	Nd	B
ASA radius (au)		4.04	2.00796	4.0205	1.9983	4.0277	2.00185
Electrons	s ↑	0.22	0.42	0.23	0.41	0.23	0.41
per atom	s ↓	0.22	0.42	0.22	0.42	0.22	0.42
per spin	p ↑	0.48	0.94	0.48	0.94	0.48	0.93
	p ↓	0.46	0.94	0.46	0.95	0.47	0.95
	d ↑	1.14		1.10		1.05	
	d ↓	1.06		1.00		0.93	
	f ↑	1.64		2.80		3.92	
	f ↓	0.46		0.42		0.38	
$N(E_F)$ (states eV^{-1}/cell)	s ↑	0.00	0.01	0.00	0.01	0.00	0.03
	s ↓	0.00	0.00	0.00	0.00	0.00	0.00
	p ↑	0.05	0.19	0.00	0.13	0.00	0.24
	p ↓	0.00	0.08	0.00	0.07	0.00	0.06
	d ↑	0.21		0.03		0.07	
	d ↓	0.16		0.13		0.12	
	f ↑	7.56		15.33		34.83	
	f ↓	0.08		0.04		0.03	
Total		8.06	0.28	15.53	0.21	35.05	0.33
Band splitting (mRyd)	s	16.2	1.3	24.7	2.4	30.9	3.1
	p	17.9	1.4	28.9	2.7	37.4	3.4
	d	21.8		36.0		48.2	
	f	64.5		388.2		529.9	
Moment per unit cell	s	0.00	−0.03	0.01	−0.05	0.01	−0.06
(μ_B)	p	0.02	−0.02	0.02	−0.05	0.02	−0.07
	d	0.08		0.10		0.12	
	f	1.19		2.39		3.53	
Total		1.24		2.41		3.53	
$\gamma(0)$ in mJ mol^{-1} K^{-2}		19.6		37.1		83.3	

Table 4. The energy difference between the paramagnetic and ferromagnetic phases for CeB_6, PrB_6 and NdB_6. ΔE is in mRyd.

Per atom	ΔE_{Band}	ΔE_{XC}	$\Delta E_{Coulomb}$	ΔE_{Mad}
Ce	62.1	−78.2	97.4	−85.4
B	12.6	−4.35	−7.85	
Pr	127.7	−161.9	201.5	−197.8
B	24.2	−8.73	−15.7	
Nd	198.2	−284.3	299.4	−300.3
B	31.8	−11.76	−21.1	

Per unit cell	ΔE_{Band}	ΔE_{XC}	$\Delta E_{Coulomb} + \Delta E_{Mad}$	Total ΔE
CeB_6	137.80	−104.29	−35.02	−1.51
PrB_6	272.75	−214.24	−90.32	−31.8
NdB_6	389.12	−354.88	−127.20	−92.9

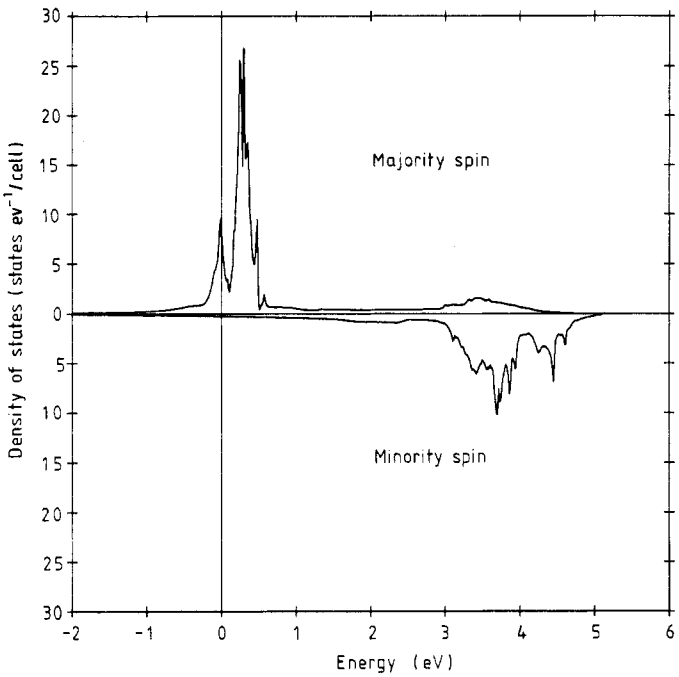

Figure 1. The cerium contribution to the density of states for spin-polarised CeB_6 near E_F.

on CeB_6 using 120 k-points rather than 84 k-points. The change in spin moment was less than 1% and even such a small stabilisation energy as 1.5 mRyd was stable to 10% between the two calculations.)

In figure 1 we show the density of states near E_F for spin-polarised CeB_6. We see that the mechanism giving the magnetism is nothing like rigid band behaviour, the states near E_F being of predominantly f character ($\simeq$90%) whilst the minority spin band roughly 3 to 4 eV above E_F is a more even admixture of f- and d-states. This contrasts with the paramagnetic case where both (degenerate) f channels are pinned to E_F with only about 10% boron p and cerium d states mixed in by hybridisation. The majority spin band resembles this paramagnetic behaviour, the only difference being that the Fermi energy moves through the little shoulder in the density of states to accommodate a surfeit of electrons of one spin-type.

3.2. Band structures and Fermi surfaces

We now turn our attention to a detailed analysis of the band structures and Fermi surfaces of each compound. Here we will present our results, leaving comparison with experiment mostly to the next section.

3.2.1. LaB_6. Figure 2(*a*) shows the band structure of LaB_6 including spin-orbit coupling in certain high-symmetry directions in the region of E_F. As we can see, the band structure

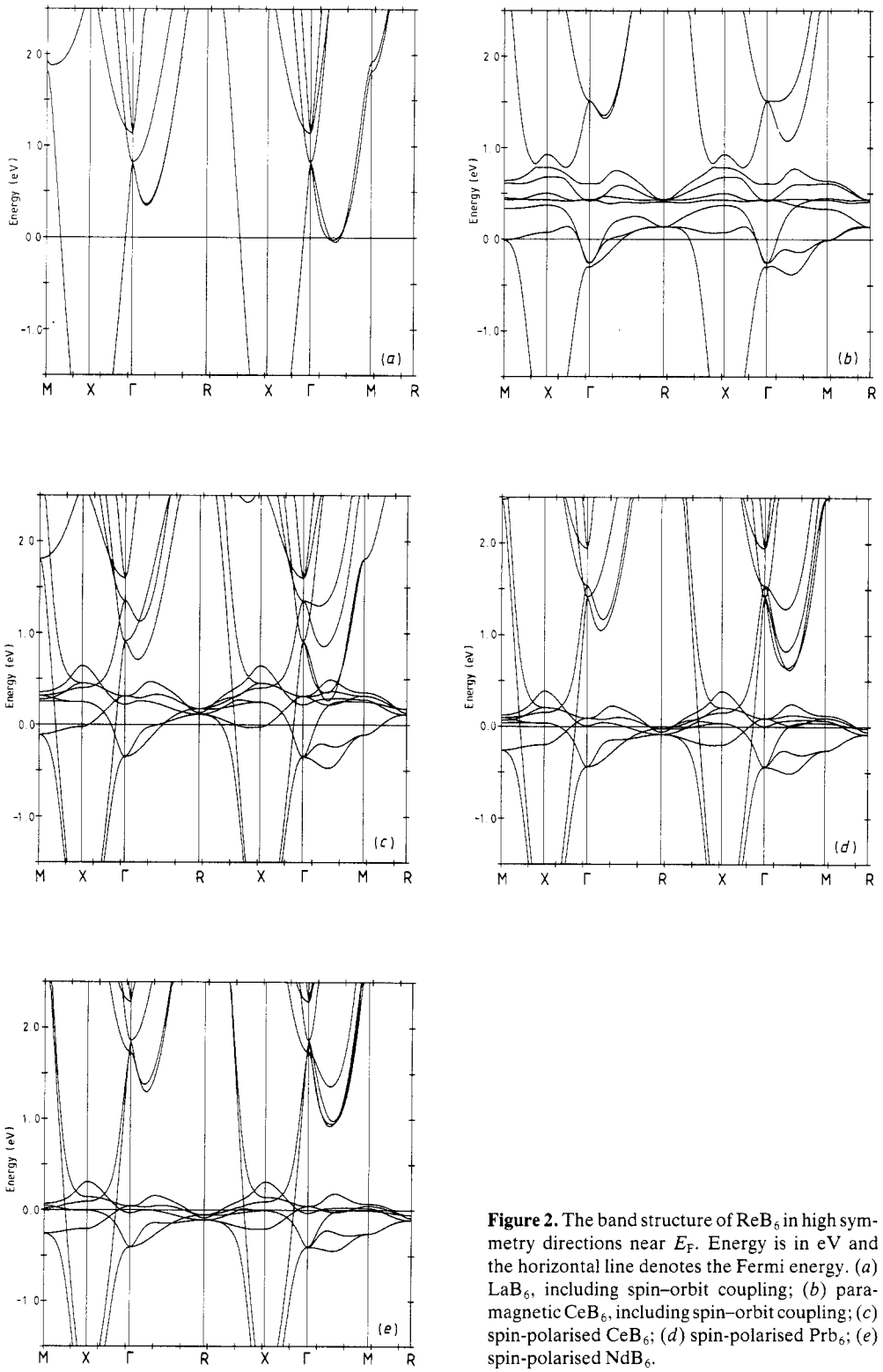

Figure 2. The band structure of ReB_6 in high symmetry directions near E_F. Energy is in eV and the horizontal line denotes the Fermi energy. (*a*) LaB_6, including spin–orbit coupling; (*b*) paramagnetic CeB_6, including spin–orbit coupling; (*c*) spin-polarised CeB_6; (*d*) spin-polarised Prb_6; (*e*) spin-polarised NdB_6.

is extremely simple, almost all of the Fermi surface being due to one broad free-electron-like band centred on the X point. This band is predominantly a d band (≃50%) with about 25% boron p and 20% La f character. Again, we interpret the La f character as being due to the re-expansion of orbitals on other sites around the La site, rather than as a real presence of f electrons.

The Fermi surface of LaB_6 is shown in figure 3(*a*). It is quite simple, consisting of ellipsoids centred on the X point and connected by necks in the (110) directions, which is in agreement both with experiment (van Deursen *et al* 1985; Onuki *et al* 1988) and previous calculations (Hasegawa and Yanase 1977). In addition we see small electron pockets in the (110) directions, which are due to another band that has a slightly greater f content. These pockets have recently been experimentally observed (Onuki *et al* 1988, 1989).

3.2.2. Paramagnetic CeB_6. Figure 2(*b*) shows the spin–orbit split paramagnetic bands near E_F for CeB_6. It is obvious that there is very little similarity between this structure and that of LaB_6. In particular, the band around the X point is ≃90% cerium f. This is due to the flat f states forcing the d band below E_F. Consequently, all the Fermi surface is mainly f character, being much more complicated (figure 3(*b*)) than that of LaB_6 and in very poor agreement with experiment (van Deursen *et al* 1985; Joss *et al* 1987; Onuki *et al* 1988 and to be published). The orbit around the X point has grown to such an extent that it touches the zone boundary along the M–R direction. (As an aside, we note that the inclusion of spin–orbit coupling only really affects the f bands at ≃½ eV above E_F—those that form the Fermi surface are almost unchanged.)

In our previous work on CeB_6, we considered the case where the cerium f electron is treated as part of the inert core of valence electrons to simulate its speculated localised nature. This calculation gave reasonable agreement with the experimental Fermi surface (figure 3(*b*)), but is totally unsatisfactory in that we are making arbitrary and unphysical assumptions about the nature of the f electrons—the fact that CeB_6 is a heavy fermion system means that the hybridisation between f electrons and other conduction electrons must be crucial, so we must include it in some way.

3.2.3. Ferromagnetic CeB_6. In figure 2(*c*) we illustrate the bands near E_F for the semi-relativistic spin-polarised calculation on CeB_6. Immediately, we notice a quite remarkable feature, namely that this band structure looks almost exactly the same as a superposition of the band structures of LaB_6 and paramagnetic CeB_6. By this we mean that there are a set of localised f bands situated near E_F in addition to the nearly free-electron-like band centred on the X point. This can be understood as follows.

In the LSD approximation to the LMTO–ASA method, the Hamiltonian reduces to two uncoupled Schrödinger equations for the two different spin directions as long as we neglect spin–orbit coupling (Gunnarsson and Lundqvist 1976). These equations are of the form

$$(-\tfrac{1}{2}\nabla^2 + V_\sigma(\boldsymbol{r}) + v_\sigma^{\mathrm{XC}}(\boldsymbol{r}))\psi_{i,\sigma}(\boldsymbol{r}) = \varepsilon_{i,\sigma}\psi_{i,\sigma}(\boldsymbol{r}) \tag{2}$$

in atomic units, where $\sigma = \uparrow$ or $\downarrow$, $V_\sigma(\boldsymbol{r})$ is the Coulomb potential and v_σ^{XC} is the exchange–correlation potential for a particular spin-type σ. The spin densities n_σ are calculated as

$$n_\sigma(\boldsymbol{r}) = \sum_{i,\,\text{occupied}} |\Psi_{i,\sigma}(\boldsymbol{r})|^2 \tag{3}$$

the only connection between spin-up and spin-down states being the requirement that

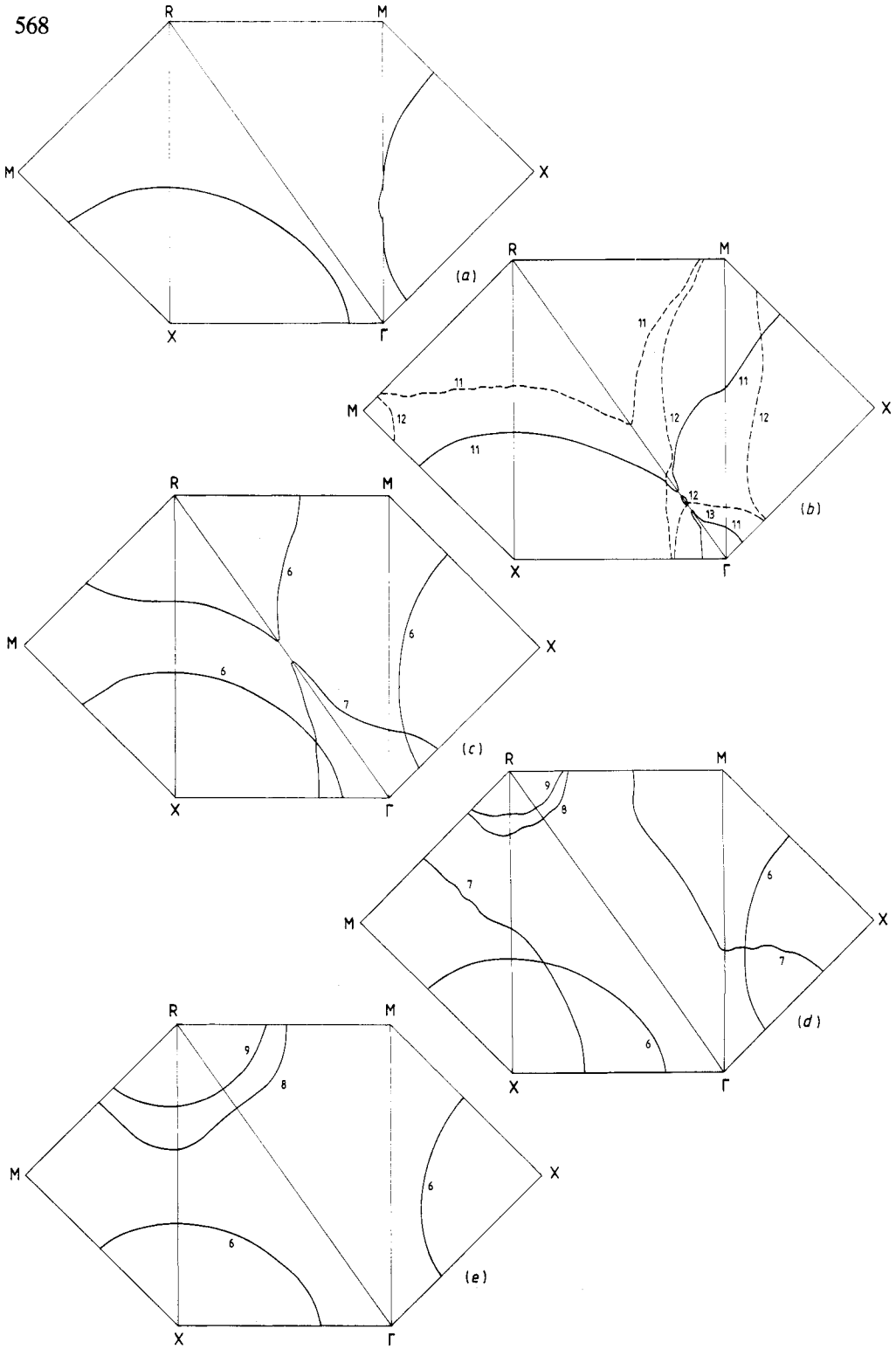

Figure 3. The fermi surfaces of ReB_6. (*a*) LaB_6, including spin–orbit coupling; (*b*) paramagnetic CeB_6 with the f states as core states (full curve) and as band states (broken curve); (*c*) spin-polarised CeB_6; (*d*) spin-polarised PrB_6; (*e*) spin-polarised NdB_6.

the sum over their occupation numbers should add up to the total number of electrons, N, i.e.

$$\int (n_\uparrow(\boldsymbol{r}) + n_\downarrow(\boldsymbol{r}))\,\mathrm{d}\boldsymbol{r} = N. \tag{4}$$

Hence, we can interpret one of these spin directions (the majority spin) as being almost exactly the same as for the paramagnetic calculation. This spin gives rise to the localised set of states at E_F, the energy density of which is very similar to that of the paramagnetic calculation, whilst the other spin direction (the minority spin) gives a diffuse set of f–d bands a few eV above E_F, rather like LaB_6, the two sets of bands not interacting. This picture is borne out if we examine the wavefunction character of the bands at E_F. The localised (majority spin) ones are $\simeq$90% f character, whilst the diffuse ones (minority spin) are above 50% d, 24% f and 24% boron p character. Hence, when we analyse the Fermi surface in figure 3(*c*), we not surprisingly see the return of the ellipsoid centred on the X point in addition to most of the Fermi surface generated by the paramagnetic calculation. This result is significant because, in this spin-polarised calculation on CeB_6, we have treated the f states as true, fully relaxed, unrestrained band states and yet we have a large portion of Fermi surface that is almost exactly the same as its non f orbital containing analogue, LaB_6. It is a very important result that, using the LMTO–ASA, which necessarily pins unoccupied f states to E_F, we have formed a Fermi surface from a very broad, dispersive band that, in analogy to LaB_6, has very little f content.

3.2.4. Ferromagnetic PrB_6. The essentially features of the band structure and Fermi surface of ferromagnetic PrB_6, illustrated in figures 2(*d*) and 3(*d*) respectively, are quite similar to those of CeB_6. Again, a paramagnetic calculation gives a Fermi surface with the X-centred orbit so large that it touches the zone boundary along the M–R direction and the whole of the Fermi surface is of predominantly f character ($\simeq$90%).

The inclusion of spin polarisation allows the broad band centred on the X point to return as a minority spin band and give rise to ellipsoids of 54% f, 19% d and 24% boron p wavefunction character. We note that this closed orbit around the X point is very stable with respect to moving the Fermi energy up or down by a few mRyd, as would be expected from the band structure. We mention this because the rest of the PrB_6 spin-polarised Fermi surface is very dependent on the precise position of E_F. This can be seen by observing the very flat bands around the R point and in M–X direction. The contribution of these bands to the Fermi surface changes vastly when we move the Fermi energy up or down by as little as 2 mRyd. Shifts of this order are usually required to get quantitative Fermi surface agreement with experiment, even for simple transition metals (Jepsen *et al* 1981), so we cannot really comment on the nature of the Fermi surface beyond the X-centred ellipsoids. Indeed, even if these flat bands did contribute to the Fermi surface, they would be extremely difficult to observe by the de Haas–van Alpen effect anyway.

3.2.5. Ferromagnetic NdB_6. Finally, we turn our attention to ferromagnetic NdB_6. We find in this case that the ferromagnetic band structure (figure 2(*e*)) again shows a dispersive band centred around the X point which gives rise to ellipsoids of Fermi surface (figure 3(*e*)) of 55% d, 16% f and 25% boron p character centred on the X point. The paramagnetic calculation pushes this dispersive band below the Fermi energy, just as in the other two compounds.

Table 5. (*a*) The theoretical de Haas–van Alphen frequency, band mass, specific heat and susceptibility for LaB_6, CeB_6, PrB_6 and NdB_6. (*b*) The experimental de Haas–van Alphen frequency, effective mass and specific heat for Lab_6, CeB_6, PrB_6 and NdB_6.

(*a*) Theory	LaB_6	CeB_6	CeB_6 ferro	PrB_6 ferro	NdB_6 ferro
F	7450	~17000	6510	5370	4410
m_{band}/m_e	0.65	1.6	0.65	0.58	0.52
$\gamma(0)$ (mJ mol^{-1} K^{-2})	1.7	23.4	19.6	37.1	83.3
$\chi_{spin}/10^{-5}$ (SI units)			8.89	1.62	1.18
$\chi_{Pauli}/10^{-5}$ (SI units)	0.68	9.48	8.16	15.21	33.99
m^*_{Theory} ratio			7.7	1.4	1.0

(*b*) Experiment	LaB_6	CeB_6	PrB_6	NdB_6
F	7810	8680	~7500	~3500
m^*_{DHVA}/m_e	0.6	6	1.8	~1.2
$\gamma(0)$ (mJ mol^{-1} K^{-2})	2.6	250	—	—

As with PrB_6, the precise nature of the predominantly f part of the Fermi surface is difficult to judge since, again, there are some extremely flat f bands around the R point and in the M–X direction, which make even a qualitative description difficult. However, the general point that the spin-polarised calculation allows a dispersive band to form around the X point is clear.

4. Comparison with experiment

In table 5(*a*) and (*b*) we show the calculated and observed extremal areas A, which are given in terms of the de Haas–van Alphen frequency F as

$$F = \hbar A/2\pi e \tag{5}$$

and the calculated band mass m_{band}/m_e and experimental effective mass m^*_{DHVA}/m_e for the orbit around the X point, on which virtually all of the experimental attention has been focused. The experimental data on LaB_6, CeB_6, PrB_6 and NdB_6 come from de Haas–van Alphen experiments (van Deursen *et al* 1985; Onuki *et al* 1988; Joss *et al* 1987; Onuki *et al* 1989), whilst there is also 2D-ACAR data on all four compounds (Tanigawa *et al* 1985).

In all these references, the similarity between the orbit around the X point in LaB_6 and the corresponding X-centred orbits in CeB_6, PrB_6 and NdB_6 has been demonstrated. Hence, we concentrate our attention on the spin-polarised calculations, where we have seen the Fermi surfaces to resemble that of LaB_6. (Table 5(*a*) and (*b*) illustrates the poor agreement obtained with the paramagnetic calculation on CeB_6 as an example.)

There is extremely good quantitative agreement for LaB_6, as one might expect for a system containing no f electrons—an upwards shift in the Fermi energy of 3 mRyd is sufficient to reproduce the observed extremal area. This level of accuracy is as good as can be expected using band theory.

The calculated de Haas–van Alphen frequencies show a trend of decreasing X-orbit area along the row of compounds, which does not account for the jump at CeB_6. The

fact that the ferromagnetic results are not in better quantitative agreement (the Fermi energy requires a shift of more than 10 mRyd for the X-centred orbit area to match the experimental data for CeB_6) could be due to the neglect of spin–orbit coupling, which gives a splitting of $\frac{1}{4}$ to $\frac{1}{2}$ eV in the paramagnetic calculation as compared with a spin splitting of 3 to 4 eV for CeB_6. The spin–orbit splitting could prove to be important even in the X-centred band as this band has a substantial f content.

It could be argued that the magnetic state we are considering does not correspond to the experimental situation. Experimentally, the ground states of CeB_6 and PrB_6 are complex antiferromagnets, whilst NdB_6 is a simple one, CeB_6 and PrB_6 having regions in the B, T phase diagram where they show antiferroquadrupolar ordering (Effantin *et al* 1985; Burlet *et al* 1988). However, it has been stated by van Deursen *et al* that, for CeB_6 at least, the high field (25 to 33 T) required to see the high mass de Haas–van Alphen oscillations gives rise to a ferromagnetic ordering with a moment of about 1 μ_B/Ce, very close to our calculated spin moment. The precise nature of the magnetic LSD ground state is unlikely to be significant because, even if the ferromagnetic state were not the LSD ground state, the fact that a field of 25 to 33 T would give a metamagnetic transition to a ferromagnetic state with moment 1 μ_B, and hence magnetic energy $\simeq$ 2 meV, means that band theory could not reliably differentiate between the two magnetic states due to their extremely small energy difference. This local ferromagnetic energy minimum has been observed as a spin flop transition in fields as low as 2 T (Horn *et al* 1981; Komatsubara *et al* 1983). van Deursen *et al* also claim that, in a de Haas–van Alphen field of 15 T, PrB_6 has a moment of 0.7 μ_B/Pr at 4.2 K, and a moment of 1.77 μ_B in zero field at 1.74 K.

Our qualitative description using the spin-polarised calculations has shown the necessity of including this large symmetry-breaking term in the Hamiltonian. In the real systems, in addition to magnetic interactions, there are crystal-field effects that further reduce the symmetry and give rise to a Γ_8 ground state (Effantin *et al* 1985; Burlet *et al* 1988). The net effect of these interactions is to split fourteen paramagnetic f states that would otherwise be pinned to the Fermi energy into a set of states lying well above E_F and a reduced number of f states still pinned to E_F, thus forcing some of the f states to be unoccupied. By including the spin-splitting (which is more important than spin–orbit splitting), we have allowed this to happen, to give a set of majority spin f bands at E_F and a diffuse set of minority spin f–d bands several eV higher in energy. As we have seen, this allows for the possibility of non-f bands at E_F and a consequent improvement in our description of the Fermi surface. We speculate that this is a general feature of f-electron systems, i.e we can get a good Fermi surface as long as we include symmetry-breaking effects in the Hamiltonian. This is well known for the classic heavy fermion system UPt_3, where there is excellent Fermi surface agreement between theory (see, for example, Wang *et al* 1987) and experiment (Taillefer *et al* 1987) as long as spin–orbit coupling is included. The spin–orbit coupling in the UPt_3 case is about 1 eV, which is about the same size as the intrinsic f bandwidth, its effect being to remove the $5f_{7/2}$ states to above the Fermi energy, leaving only the $5f_{5/2}$ states to contribute to the Fermi surface. In this case, it is the platinum s–p–d states that are important for the broader bands around the Fermi energy (Christensen *et al* 1989).

5. Enhancements

Finally we come to the question of enhancements, i.e. by what factor the de Haas–van Alphen electron masses m^*_{DHVA} and low temperature specific heats $\gamma(0)$ are enlarged

over their band theory values. We will divide this section into two parts. First, there will be a discussion of the enhancements determined by comparing the experimental data with our results and secondly there will be a theoretical interpretation based on our calculations.

5.1. Experimental

As we can see, the theoretical de Haas–van Alphen masses m_{band}, calculated as

$$m_{\text{band}} = (\hbar^2/2\pi)\,\partial A/\partial E \tag{6}$$

are in very poor agreement for CeB_6 indicating that the bands at the Fermi energy should be much flatter than those we have calculated. The enhancement in m^*_{DHVA} is about 2 to 3 for PrB_6 and NdB_6, but comparison with experiment for CeB_6 is complicated by the fact that m^*_{DHVA} is a function of external magnetic field (Joss *et al* 1987; Springford and Reinders 1988; Onuki *et al* 1989). Onuki *et al* extrapolate a zero-field value of $m^*_{\text{DHVA}} \simeq 15$, giving an enhancement over our calculated value of about 25. An enhancement of this size is always found with band theory studies of heavy fermion systems, indicating the existence of many-body effects not included in the LSD approximation. Our results and experiment also indicate that this factor of 25 is roughly the amount by which m^*_{DHVA} is increased in CeB_6 relative to the non f-containing LaB_6.

However, when we turn our attention to the specific heat, we notice that the experimental $\gamma(0)$ for CeB_6 is about 100 times larger than the experimental $\gamma(0)$ for LaB_6 and about 11 times larger than our theoretical $\gamma(0)$ for CeB_6. If we analyse the linear specific heat coefficient for CeB_6 as

$$\gamma_{\text{Expt}}(0) = \gamma_{\text{Theory}}(0)(1 + \lambda) \tag{7}$$

where $\gamma_{\text{Theory}}(0)$ is the free-electron value given in terms of the total density of states at E_F, $N(E_F)$, as

$$\gamma_{\text{Theory}}(0) = (\pi^2 k_B^2/3)N(E_F) \tag{8}$$

we obtain an enhancement in the specific heat of $\lambda \simeq 10$ if the f electrons are included in the $N(E_F)$ and $\lambda \simeq 150$ without the f contribution.

Experimentally, there appears to be a discrepancy between the mass enhancement of 25 determined for the X-centred orbit by the de Haas–van Alphen effect and the mass enhancement of 100 inferred from the specific heat (Springford and Reinders 1988). Within the context of our calculations, this is not a difficulty. This is because the Fermi surface is formed by two very distinct sets of bands—a broad d-state minority spin set and a very narrow f-state majority spin set. We can then postulate that, experimentally, only the minority spin part of the Fermi surface has been seen and that the majority spin part, due to its high f content, possesses a much larger enhanced de Haas–van Alphen effective mass. This could bring m^*_{DHVA} averaged over all the Fermi surface inline with the enhancement determined from the low temperature specific heat. This possibility of electrons of different spin-types contributing to different parts of the Fermi surface has also been suggested by Onuki *et al* (1989). It should be mentioned, however, that the de Haas–van Alphen effect probes only the itinerant electrons and is insensitive to local effects, so that low temperature specific heat may show contributions from the entropy of the local f moments. As a result, deviations between the $\gamma(0)$ and de Haas–van Alphen derived effective masses may be seen at lower fields where the phase transition from antiferromagnetic to quadrupolar ordering is observed in the specific heat (Effantin *et al* 1985; Bredl 1987).

5.2. Theoretical

We now turn our attention to a theoretical interpretation of the observed mass enhancement in terms of an enhancement in the spin susceptibility χ_{spin}. To do this, we consider the stabilisation energy of the magnetic ground state ΔE and the spin moment M and calculate χ_{spin} by writing the Landau free energy of a ferromagnet (Landau and Lifshitz 1959) ΔE (at $T = 0$) as

$$\Delta E = (a/2)M^2 + (b/4)M^4. \tag{9}$$

By using our calculated values of ΔE and M we can evaluate the coefficients a and b from the condition that the free energy by a minimum. From this we can find χ_{spin} as

$$1/\chi_{spin} = -\partial^2 \Delta E/\partial M^2 = 8\Delta E/M^2. \tag{10}$$

Converting to SI units, we have

$$\chi_{spin} = \mu_0 V M_V^2/8\Delta E \tag{11}$$

where V is the unit cell volume and M_V the magnetisation density. We quote our calculated values of χ_{spin} in table 5(a). It should be noted that the Landau expression for the free energy assumes that the order parameter M is small and that we are close to the critical temperature T_C. Neither of these conditions is satisfied in this case, so we will use the calculated values of χ_{spin} to be indicative of the relative values of the susceptibility in these systems. In table 5(a) we also show the Pauli susceptibilities χ_{Pauli}, calculated as

$$\chi_{Pauli} = \mu_0 \mu_B^2 N(E_F). \tag{12}$$

As we can see, χ_{Pauli} is very similar to χ_{spin} for CeB_6, and an order of magnitude bigger for PrB_6 and NdB_6. We can remove this obstacle for the praseodymium and neodymium compounds by arguing that their huge values of χ_{Pauli} are due to the fact that they do not form saturated ferromagnetic states, even in high de Haas–van Alphen magnetic fields, so we are not looking at even a metastable state of these systems. There is probably not a large energy difference between the ferromagnetic states of these compounds and their observed ground states, but the interactions we have neglected could certainly result in a drastic reduction in their densities of states—we are far more justified in believing that ΔE and M are fairly insensitive to the precise nature of the LSD ground state because they are evaluated in terms of integrals over the whole Brillouin zone. This sensitivity of the density of states if best illustrated by a calculation on SmB_6. In the paramagnetic phase, our calculations indicated a very large value of $N(E_F) = 69.9$ states eV^{-1} cell. However, the inclusion of spin–orbit coupling allowed a very small energy gap to open up, due to the $j = 7/2$ states being pushed above E_F. Thus $N(E_F)$ was reduced to zero while the f-electron count changed by about 0.2%. The value of the energy gap was dependent on the sphere sizes, but we could place it as being in the region of 3 to 10 meV. The existence of this (very small) energy gap confirms the experimental observation that SmB_6 is a small gap semiconductor (Allen *et al* 1979).

In spite of these restrictions, we tentatively calculate a theoretical effective mass ratio as

$$m^*_{CeB_6}/m^*_{PrB_6} = \chi_{spin,CeB_6}/\chi_{spin,PrB_6} \tag{13}$$

etc. We give these ratios in table 5(a) and, as we can see, we can indeed interpret CeB_6 as having an enhanced effective mass relative to PrB_6 and NdB_6.

This is a good result for the LSD. LSD does include exchange–correlation effects, but it does not take into account the dynamics of the self-energy of the quasi-particles on the Fermi surface, hence the observation that the slope of the bands is too small. However, these effects should only be important on an energy scale that characterises the heavy fermion coherence temperature T^*. This is usually of the order of 10 K, i.e. $\simeq$ 1 meV, the heavy fermion compound CeB_6 having a Kondo temperature of 2 K (Onuki *et al* 1989). Hence, we can in principle calculate the energy difference between the paramagnetic and ferromagnetic states accurate to a few meV even if we do not treat the quasiparticles correctly. This means that ΔE and M must be reasonably well described quantities, so an analysis using these parameters is justifiable.

It should be pointed out that we can comment on the quasiparticles because we have considered an excited state in our calculation, i.e. the paramagnetic state. However, this excited state is in fact the ground state of a constrained system in which we do not allow any magnetism to occur. This idea of using DFT (which necessarily treats only the ground state exactly (Hohenberg and Kohn 1964)) to analyse excited state properties by transforming the excited state into the ground state of a constrained system has also been used to predict the 3d excitation spectra in NiO (Norman and Freeman 1986) and to calculate an effective Hamiltonian for La_2CuO_4 (McMahan *et al* 1988).

6. Conclusions

We have shown that the rare-earth hexaborides CeB_6, PrB_6 and NdB_6 form energetically stable magnetic states within the LSD band theory formalism.

From analysis of these magnetic states, and by comparison with the non f-orbital containing isostructural analogue LaB_6, we have found that, although the f states are responsible for almost all of the magnetism and a part of the Fermi surface, there is still a large non-f wavefunction component at the Fermi energy, even with the majority spin f states pinned there. This wavefunction gives rise to a broad band centred on the X point of the Brillouin zone, from which derives that part of the Fermi surface that has been experimentally observed. We find qualitative agreement with experiment for the extremal orbit areas, but not for the de Haas–van Alphen masses, indicating that there are important many-body effects present that we are not taking into account. However, throughout our calculations, we observe that the heavy fermion compound CeB_6 is indeed very different to moderately enhanced PrB_6 and NdB_6.

First, CeB_6 exhibits a much greater degree of hybridisation between f and s–p–d states, as shown by the electron count and relative band positions. Secondly, in the magnetic state, the spin splitting of the f states is relatively very small for such a large spin moment. This fact leads to a small magnetic stabilisation energy, which, as we have shown using simple Landau theory, can be interpreted as an enhancement in the spin susceptibility and hence an enhancement in the effective mass averaged over all the Fermi surface.

Hence, we have obtained a good description of the Fermi surface and an indication of the origin of the enhancements for the Kondo lattice CeB_6 using a fully self-consistent band theory calculation which treats the f electrons as true conduction band states. We believe that this is the first time that the Fermi surface of a heavy fermion cerium compound has been calculated correctly using a conventional local density calculation.

References

Allen J W, Batlogg B and Wachter P 1979 *Phys. Rev.* B **20** 4807

Andersen O K 1975 *Phys. Rev.* B **12** 3060

Anderson P W 1961 *Phys. Rev.* **124** 41

Blum P and Bertaut F 1954 *Acta Crystallogr.* **7** 81

Bredl C D 1987 *J. Magn. Magn. Mater.* **63–4** 355

Burlet P, Effantin J M, Rossat-Mignod J, Kunii S and Kasuya T 1988 *Proc. Int. Conf. Magnetism (Paris, 1987)*

Christensen N E, Andersen O K, Gunnarsson O and Jepsen O 1988 *J. Magn. Magn. Mater.* **76–7** 23

van Deursen A P J, Pols R E and de Vroomen A R 1985 *J. Less-Common Met.* **111** 331

Effantin J M, Rossat-Mignod J, Burlet P, Bartholin H, Kunii S and Kasuya T 1985 *J. Magn. Magn. Mater.* **47–8** 145

Gunnarsson O and Lundqvist B I 1976 *Phys. Rev.* B **13** 4274

Hasegawa A and Yanase A 1977 *J. Phys. F: Met. Phys.* **7** 1245

Hohenberg P and Kohn W 1964 *Phys. Rev.* **136** 864

Horn S, Staglich F, Loewenhaupt M, Scheuer H, Felsch W and Winzer W 1981 *Z. Phys.* B **42** 125

Jepsen O, Glötzel D and Mackintosh A R 1981 *Phys. Rev.* B **23** 2684

Joss W, van Ruitenbeek J M, Crabtree G W, Tholence J L, van Deursen A P J and Fisk Z 1987 *Phys. Rev. Lett.* **59** 1609

Kohn W and Sham L J 1965 *Phys. Rev.* **140** 1133

Komatsubara T, Sato N, Kunii S, Oguro I, Furukawa Y, Onuki Y and Kasuya T 1983 *J. Magn. Magn. Mater.* **31–4** 368

Landau L D and Lifshitz E M 1959 *Statistical Physics* (Oxford: Pergamon)

Langford H D and Temmerman W M unpublished

Langford H D and Temmerman W M 1988 *J. Magn. Magn. Mater.* **76–77** 43

McMahon A K, Martin R M and Satpathy S 1988 *Phys. Rev.* **B38** 6650

Morruzzi V L, Janak J F and Williams A R 1978 *Calculated Electronic Properties of Metals* (Oxford: Pergaon)

Norman M R and Freeman A J 1986 *Phys. Rev.* B **33** 8896

Oguchi T and Freeman A J 1985 *J. Magn. Magn. Mater.* **52** 174

—— 1986 *J. Magn. Magn. Mater.* **61** 233

Onuki Y, Kurosawa Y, Omi T, Komatsubara T, Yoshizaki R, Ikeda H, Maezawa K, Wakabayashi S, Umezawa A, Kwok W K and Crabtree G W 1988 *J. Magn. Magn. Mater.* **76–7** 37

Onuki Y, Komatsubara T, Reinders P H P and Springford M 1989 unpublished

Pickett W E 1986 Relationship of band theory to heavy fermion behaviour *Proc. Int. Sch. Electronic Band Structure and its Applications (Kanpur, 1986)*

Rasul J W and Desgranes H-U 1986 *J. Phys. C: Solid State Phys.* **19** L671

Schönhammer K and Gunnarsson O 1988 *Phys. Rev.* B **37** 3128

Skriver H L 1984 *The LMTO Method (Springer Series in Solid State Sciences 41* (Berlin: Springer)

Springford M and Reinders P H P 1988 *J. Magn. Magn. Mater.* **76–7** 11

Stewart G R 1984 *Rev. Mod. Phys.* **56** 755

Stewart G R, Fisk Z, Willis O and Smith J L 1984 *Phys. Rev. Lett.* **52** 679

Taillefer L, Newbury R, Lonzarich G G, Fisk Z and Smith J L 1987 *J. Magn. Magn. Mater.* **63–4** 372

Tanigawa S, Terakodo S, Ito K, Morisue A, Komatsubara T, Onuki Y and Shiotani N 1985 *Positron Annihilation* ed P C Jain *et al* (Singapore: World Scientific)

von Barth U and Hedin L 1972 *J. Phys. C: Solid State Phys.* **5** 1629

Wang C S, Norman M R, Albers R C, Boring A M, Pickett W E, Krakauer H and Christensen N E 1987 *Phys. Rev.* B **35** 7260